Journal of Membrane Science 573 (2019) 309–319

Contents lists available at ScienceDirect

Journal of Membrane Science

journal homepage: www.elsevier.com/locate/memsci

A novel gold nanocomposite membrane with enhanced permeation, rejection and self-cleaning ability

Milad Rabbani Esfahani[a,*], Negin Koutahzadeh[b], Amirsalar R. Esfahani[c], Mostafa Dadashi Firouzjaei[a], Benjamin Anderson[a], Lauren Peck[a]

[a] Department of Chemical and Biological Engineering, University of Alabama, Tuscaloosa, Al 35487, United States
[b] Ralph E. Martin Department of Chemical Engineering, University of Arkansas, Fayetteville, AR 72701, United States
[c] Center for the Management, Utilization and Protection of Water Resources, Tennessee Technological University, Cookeville, TN, 38505, United States

ARTICLE INFO

Keywords:
Mixed matrix membrane
Natural organic matter
Water treatment
Anti-fouling
Catalytic behavior

ABSTRACT

The trade-off relationship between permeability, selectivity, and antifouling capability of nanocomposite membranes is the focal point of effective membrane technology. This study introduces a new gold nanocomposite membrane with enhanced antifouling behavior and permeability, as well as improved rejection capability for water treatment. Different (0.5, 1 and 2 wt%) concentrations of citrate-stabilized (coating) gold nanoparticles (CT-GNPs) having a core size of 50 nm were embedded into the polysulfone (PSF) membranes by the phase inversion method, resulting in alterations on PSF membrane performance. The intrinsic physicochemical properties and operational ability of all gold nanocomposite membranes were evaluated with regard to the self-cleaning, flux and selectivity criteria for water purification process. The PSF/0.5% GNPs demonstrated the optimal pore structure, morphology, and electrochemical surface properties among the gold nanocomposite and pure PSF membranes. The negative surface charge and the super hydrophilic functional group of CT-GNPs enhanced the permeation (at least three times in comparison with pure PSF membranes) and rejection ability of nanocomposite membranes. In addition, CT-GNPs showed digestive behavior towards humic acid (HA), a natural foulant, that significantly enhanced the antifouling ability (FRR = 95%) of the gold nanocomposite membranes by degrading the HA formed cake layer on the membrane surface and fragmenting the large HA aggregates that blocked the pores. The degradation of HA compounds by the embedded CT-GNPs occurred during the filtration process at room temperature and under the regular visible light. The stability of embedded GNPs into the polymeric matrix of membranes was evaluated at static and dynamic conditions for several days, and no release of CT-GNPs was observed.

1. Introduction

The scarcity of water resources and the increasing rate of water contamination by humans and industrial wastes have highlighted water and wastewater purification as a major global issue for all countries [1,2]. The Membrane technology as a promising solution for water treatment has shown incredible performance due to the low cost of fabrication, reliability, flexibility, and replicability of the process [3]. Nanocomposite membranes, as the new generation of polymeric membranes, have shown the potential properties to minimize the limiting factors that have held polymeric membranes back from being effective water treatment agents. The mixed matrix membranes (MMMs) are polymeric membranes embedded with nanoparticles (NPs) that enhance the mechanical, physio-chemical and operational properties of membranes. The effectiveness of nanoparticles as the modifier agent relies on concentration, dispersion and physicochemical properties of NPs, such as functional group and electrical surface charge [4]. The optimization of nanocomposite membrane properties tailored to meet the demands for water treatment includes incorporating high permeability, high selectivity, and enhanced anti-fouling characteristics. Both physical modification of membrane structural characteristics such as pore size [5], porosity [6], and thickness [7], as well as optimization of operational parameters such as pressure and flow [8,9], can improve membrane performance. However, modification of membrane physicochemical properties using the power of nanoparticles is an approach that brings all the mentioned features to the nanocomposite membranes. Different nanoparticles, such as graphene oxide (GO) [10], silicon dioxide (SiO_2) [11], ferrous ferric oxide (Fe_3O_4) [12], silver [13]

* Corresponding author.
E-mail address: mesfahani@eng.ua.edu (M.R. Esfahani).

https://doi.org/10.1016/j.memsci.2018.11.061
Received 23 August 2018; Received in revised form 26 October 2018; Accepted 24 November 2018
Available online 29 November 2018

and titanium dioxide [14] have been used as the modifier agent to improve membrane performance in terms of permeability, rejection and antifouling capability. However, the performance of nanocomposite membranes is still limited by the trade-off relationship between permeability, selectivity and antifouling capability. The best candidate additive should improve all three mentioned properties without compromising or negatively affecting any others. Therefore, the current need is to develop membranes with high permeability, improved self-cleaning ability and high rejection for water purification under the context of energy efficiency and cost-effectiveness [15]. The other main concern surrounding nanocomposite membranes is their durability, and the stability of embedded nanoparticles into the membrane matrix [16,17]. One negative feedback point about the nanocomposite membranes is leaching of nanoparticles after a short time of operation, or during the membrane cleaning process [18]. Therefore, the best nanoparticle candidate for fabrication of nanocomposite membranes can 1.) Improve all three of permeability, antifouling and rejection ability of membranes, and 2.) Has strong stability and functionality inside the polymeric membrane.

Gold nanoparticles (GNPs) possess unique optical and electronic properties that can be used for different fields of application, such as sensors, catalysis, electronics, photonics, solar cells, cancer diagnosis/therapy, drug delivery and biomedical imaging [19]. One advantage of GNPs is that they can be adapted to certain applications based on the modification of optical and electronic properties by changing their size, shape, surface chemistry, or aggregation state [20]. Recently, a new ability of GNPs as antioxidants and anti-coagulants was reported by Lundin et al. [19]. Pallem et al. described the interaction of humic acid (HA) and GNPs as a function of compatibilizer composition [21]. In our previous studies [22–24], we showed that citrate-coated GNPs (CT-GNP) in size of 50 nm disaggregated the HA aggregates at room temperature. It was postulated that disassociation of HA aggregates in the presence of CT-GNPs is due to the interference of GNPs with loose bounds of HA aggregates. The main advantage of HA degradation process by CT-GNPs was that the process occurred at room temperature and regular visible light, with no need of activation process [22]. Membrane fouling by natural organic matters (NOM) has been known as one of the main limiting factors of membrane processes that deteriorates the efficiency of the membranes; thus, the degrading ability of GNPs towards HA can be used as the self-cleaning agent [25,26]. In general, NOM fouling initiates by deposition and attachment of organic matters on the surface and pores of the membranes. This phenomenon prevents water from passing through the membrane channels, and as a result, reduces the water flux and affects the rejection mechanism of the membrane [27]. NOM such as humic acid (HA) and fulvic acid can be addressed as the predominant foulants in water and wastewater treatment [28]. The carboxylic (COOH), phenolic substituents (OH), and methoxy carbonyls (C=O) in aromatic nuclei form the main structure of HA. This structure not only provides an appropriate structure to interact with the membrane surface, but also facilitates reaction and attachment to other agents such as metallic ions that results in more severe fouling [29,30]. Based on the fouling mechanism of HA and digestive ability of GNPs towards HA at room temperature and under the regular visible light, GNPs have noticeable ability to act as an antifouling agent for water purification process. In addition, CT-GNPs have three hydrophilic carboxylic and hydroxyl groups on the surface that can improve the hydrophilicity of membranes and therefore improve the water flux [31–33].

In this study, for the first time, the mixed matrix membranes using CT-GNPs were fabricated and tested for water purification The water flux, self-cleaning ability, and HA rejection of the gold nanocomposite membranes were evaluated at different concentrations of CT-GNPs via cross-flow filtration process. The direct effect of embedded CT-GNPs on HA aggregates (foulant) were studied and used as the index of antifouling capability. Finally, the stability of embedded CT-GNPs into the polysulfone matrix of membranes were examined at both static and several dynamic operational conditions.

2. Materials and methods

2.1. Materials

CT-GNPs having a core size of 50 nm were purchased from Ted Pella, Inc. (Redding, CA, USA) in aqueous dispersions. Polysulfone Udel P-3500 LCD MB7 (PSF) (molecular weight (MW): 77–83 kg/mol) was provided by Solvay Advanced Polymers (Alpharetta, GA, USA). Humic acid sodium salt, (HA) and N-Methyl-2-pyrrolidinone (NMP), were purchased from Sigma-Aldrich (St. Louis, MO, USA). The necessary deionized (DI) water for membrane fabrication and filtration processes was produced from the Millipore DI system Direct-Q 3 UV (Massachusetts, USA) (18.2 MΩ cm).

2.2. Preparation of gold nanocomposite membranes

The mixed matrix membranes were prepared via the phase inversion (PI) method. To prepare the casting solution, first, the specific amount of 0.5, 1, and 2 (wt%) CT-GNPs were added to NMP and stirred for 30 min to produce a well-dispersed solution. Then, the solution was sonicated at 25 °C for 30 min using ultrasonic bath (120 V, 50/60 Hz). Finally, 15 g (wt%) of PSF powder was gradually added to the casting solution and stirred for 12 h to ensure the dissolution of PSF. The prepared casting solution was rested for 12 h to allow a complete release of bubbles. The casting solution was cast using a casting knife at the thickness of 210 μm on a clean glass sheet. The casted film was exposed to atmospheric air for 30 s and was then immersed in DI water (coagulation bath) until the formed membrane was peeled off from the glass (Fig. 1). Finally, membranes were washed with DI water and were kept in DI water for at least 12 h before initiating the filtration process.

2.3. Characterization techniques

Structural and physicochemical characterization of membranes: The rheological behavior of the membranes casting solutions were analyzed using RVDV2T viscometer (Brookfield, Middleboro MA, USA). The morphology of the prepared gold nanocomposite and PSF membranes was investigated by studying the cross sections of the membranes using scanning electron microscope (SEM) (JEOL 7000 FE SEM, Peabody, MA, USA). Fourier transform infrared spectroscopy (FTIR) (Bruker Vertex 70, USA) was used for verification of the presence of GNPs in gold nanocomposite membranes at ambient temperature. The spectra were collected between wave numbers of 4000–400 cm^{-1} and the result of 256 scans at a resolution of 2 cm^{-1} was reported.

Both the static and dynamic pure water contact angle (CA) of the membranes surface were determined by using Theta Lite Optical Tensiometer (Biolin Scientific Inc., Paramus, NJ, USA). For static contact angle measurement, 1 μL water droplets were placed at different positions on the membrane surface for replication. The average value of at least five measurements was reported. The dynamic contact angle measurement was evaluated by placing 1 μL water droplets on the membrane surface using an automated syringe and recording the changes of contact angle as a function of drop age for 2 min.

The electrical surface charge of the membranes was measured using the surface zeta potential cell of the Zetasizer Nano ZS (Malvern Instruments Ltd, Malvern, United Kingdom). The 0.2 μm polystyrene latex (Polysciences Inc., PA, USA) was used as the tracer for all the measurements [34].

In order to determine the overall porosity of the membranes, the gravimetric method formulated in Eq. (1) [35] was used.

$$\varepsilon = \left(\frac{W_{wet} - W_{dry}}{A \times l \times \rho_w} \right) \quad (1)$$

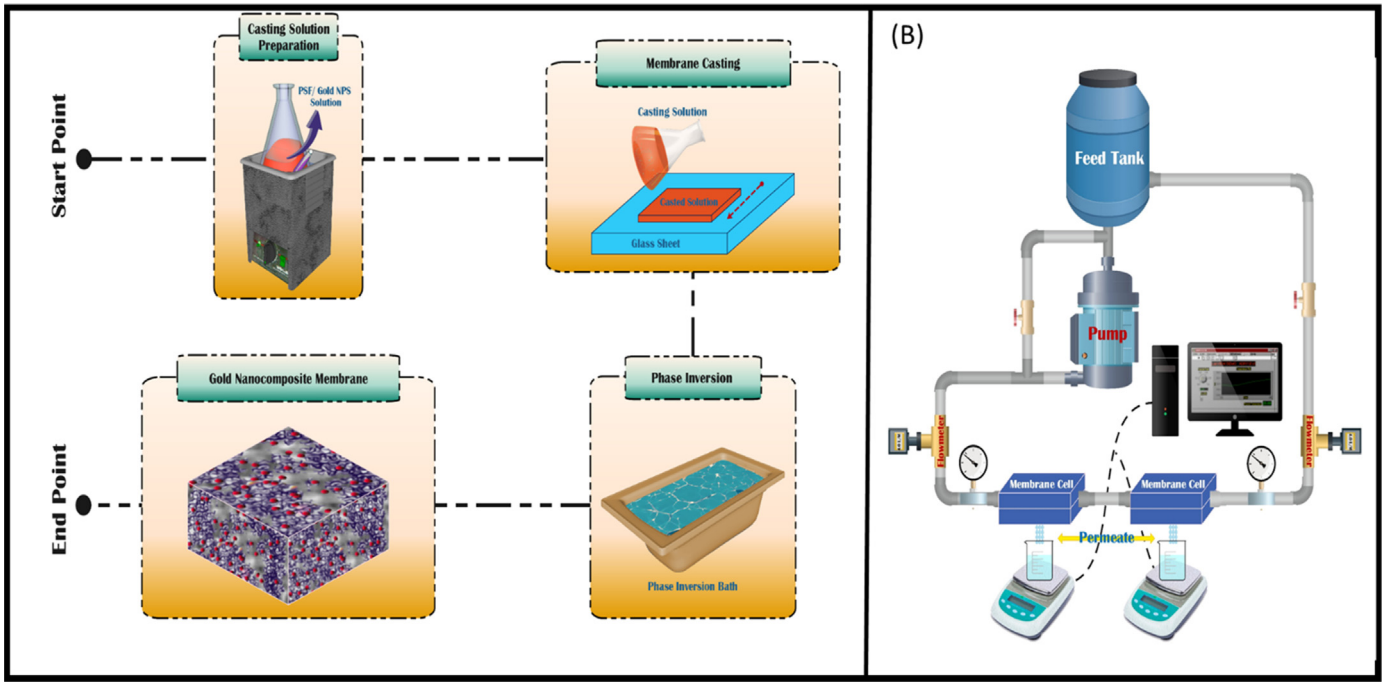

Fig. 1. (a) Schematic flow chart of the gold nanocomposite membranes fabrication process, (b) Schematic diagram of cross-flow ultrafiltration experimental apparatus.

here W_{wet} stands for the weight of the membrane after 3 days of immersion in DI water, W_{dry} stands for weight of membrane after 12 h drying at the 80 °C. *A*, *l*, and ρ_w are membrane effective area (m^2), membrane thickness (m), and water density (g cm^{-3}), respectively.

2.3.1. Pure water permeation, HA filtration, antifouling and rejection of the membranes

A cross-flow filtration process was employed to evaluate the water permeation, filtration and HA rejection of all membranes (Fig. 1). Two membrane cells at transmembrane pressure (TMP) of 0.16 MPa and velocity of 0.16 m s^{-1} empowered by the gear pumps were used for filtration experiments. The permeate of the membranes was measured using two laboratory mass balances under the membrane cells connected to the computer. All the membranes were compacted at TMP of 0.3 MPa for 1 h to achieve stable flux before conducting the permeation tests. Water flux of the membranes calculated using Eq. (2). At least three membrane samples were tested for each experiment, and the average value was reported.

$$J_{w1} = \frac{V}{A \times \Delta t} \tag{2}$$

here, J_{w1}, V, A, and Δt stand for pure water flux (L.m^{-2}.h^{-1}), permeate water volume (L), membrane effective surface area (m^2), and filtration time (h).

Antifouling properties of the membranes evaluated based on the flux recovery ratio (FRR%) using Eq. (3):

$$FRR = \left(\frac{J_{w2}}{J_{w1}}\right) \times 100 \tag{3}$$

FRR % is the index for the antifouling ability of the membrane regarding hydraulic cleaning process. In this process, first water flux (J_{w1}) was calculated as described in the filtration test. Then, HA solution (10 ppm) was filtered at TMP of 0.16 MPa and cross-flow velocity of 0.16 m s^{-1} for 2 h. After completion of HA filtration, the membranes were washed at the atmospheric pressure and cross-flow velocity of 0.16 m s^{-1} for 15 min. Finally, pure water flux after the cleaning process (J_{w2}) was calculated at the TMP of 0.16 MPa and cross-flow velocity of 0.16 m s^{-1}. The average amount of the FRR % was reported from at least three different membrane samples for each type of pure PSF and gold nanocomposite membrane.

In order to analyze the reversibility and irreversibility of membrane fouling behavior, the fouling ratio was determined using the following equations:

$$\%R_t = \left(1 - \frac{J_{HA}}{J_{w1}}\right) \times 100 \tag{4}$$

$$\%R_r = \left(\frac{J_{w2} - J_{HA}}{J_{w1}}\right) \times 100 \tag{5}$$

$$\%R_{ir} = \left(\frac{J_{w1} - J_{w2}}{J_{w1}}\right) \times 100 \tag{6}$$

where $\%R_t$, J_{HA}, R_r, and R_{ir} are the total fouling ratio, HA flux, reversible fouling ratio, and irreversible fouling ratio, respectively. These experiments were performed for at least three separate membrane samples and the average value was reported. Organic carbon measurements were conducted using a Shimadzu TOC-VCPH total organic analyzer (Shimadzu Scientific Instruments, Columbia, MD, USA).

2.3.2. Antifouling activity of CT-GNPs

The particle size distribution and zeta potential of CT-GNPs (before adding to the casting solution) were evaluated based on dynamic light scattering (DLS) approach by the zetasizer Nano ZS (Malvern Instruments Ltd, Malvern, United Kingdom) [36,37]. To evaluate the effect of CT-GNPs on fouling, the particle size and particle size distribution of HA particles were measured in both the feed stream (suspension) - (10 ppm HA) and the permeate stream after 5, 30 and 60 min of filtration using pure PSF and gold nanocomposite membranes. The HA aggregates behavior in the permeate streams of all the membranes were compared with HA aggregates behavior in the feed stream. In parallel analysis, the HA aggregates pattern in permeate stream of gold nanocomposite membranes were compared with the HA aggregates pattern in permeate stream of pure PSF membranes to evaluate the effect of CT-GNPs on HA fouling.

2.3.3. GNPs stability in PSF polymeric matrix

The stability and durability of embedded CT-GNPs into the polymeric matrix was evaluated using static and dynamic experiments. In the static condition, the gold nanocomposite membranes were kept in clean containers filled with DI water for more than three months, and possible release of GNPs from gold nanocomposite membranes into the DI water were checked regularly by analyzing the samples of stored DI water using UV–Vis spectrophotometer (GENESYS™ 10S, Thermo Scientific, USA). UV–visible extinction spectra were recorded from 200 to 800 nm using a quartz cuvette having a 1 cm path length. In the dynamic condition, the release of CT-GNPs were monitored during the filtration test at two TMP of 0.16 MPa and 0.3 MPa and cross-flow velocity of 0.16 m s^{-1}, the same condition for the filtration tests. For dynamic stability experiments, gold nanocomposite membranes were placed in the membrane cells at the mentioned operational conditions and different samples were taken regularly from the permeate stream during the filtration test for two weeks. The samples were analyzed for possible leaching out of CT-GNPs in the permeate stream using the UV–Vis spectrophotometer.

3. Results and discussions

3.1. Membrane structure, morphology and surface properties

Fig. 2 shows SEM images of membrane cross-sections that visualized membrane pore morphology. A careful examination of SEM images highlights two general main characteristic differences between the pure PSF and gold nanocomposites membranes: 1) The pure PSF membranes have a thick top layer with relatively few pores, but the top layer of all the gold nanocomposite membranes are thinner with a higher number of pores under it, 2) The pure PSF membranes consist of spherical non-connected pores with thick walls, but the gold nanocomposite membranes possess small finger-like pores near the top layer and sponge-like pores in the sub-layer. The top surface pores analysis of the membranes (Fig. 3) shows that all the membranes possess the same pore size range while the number of smaller pores (< 40 nm) increased for all the gold nanocomposite membranes in comparison to pure PSF. The change of pore size and pore morphology can be explained based on the competitive thermodynamics and kinetics process during the phase inversion process [38]. In general, if added nanoparticles work as a non-solvent agent and reduce the thermodynamic miscibility of the casting solution, this condition leads to the enhanced rapid mixing which results in the finger-like pore morphology. On the other hand, if added nanoparticles increase the casting solution viscosity, then the delayed demixing is achieved that results in sponge-like pore morphology [39,40]. In the fabrication of gold nanocomposite membranes, the changes of membrane structure are a combination of both mentioned factors. - The viscosity of casting solutions was increased to 567 and 600 (cP) by adding the 0.5% and 1% (wt%) GNPs into the casting solution in comparison to the viscosity of pure PSF casting solution (519 cP). Therefore, the formation of the sponge-like sub-layer structure in PSF/0.5% GNP and PSF/1% GNP can be attributed to the delayed demixing process created due to the higher viscosity of the casting solutions. However, the effect of CT-GNPs at higher concentration (2 wt%) on thermodynamic instability (miscibility) conquered the viscosity effect and led to rapid demixing phase separation resulting in long finger-like

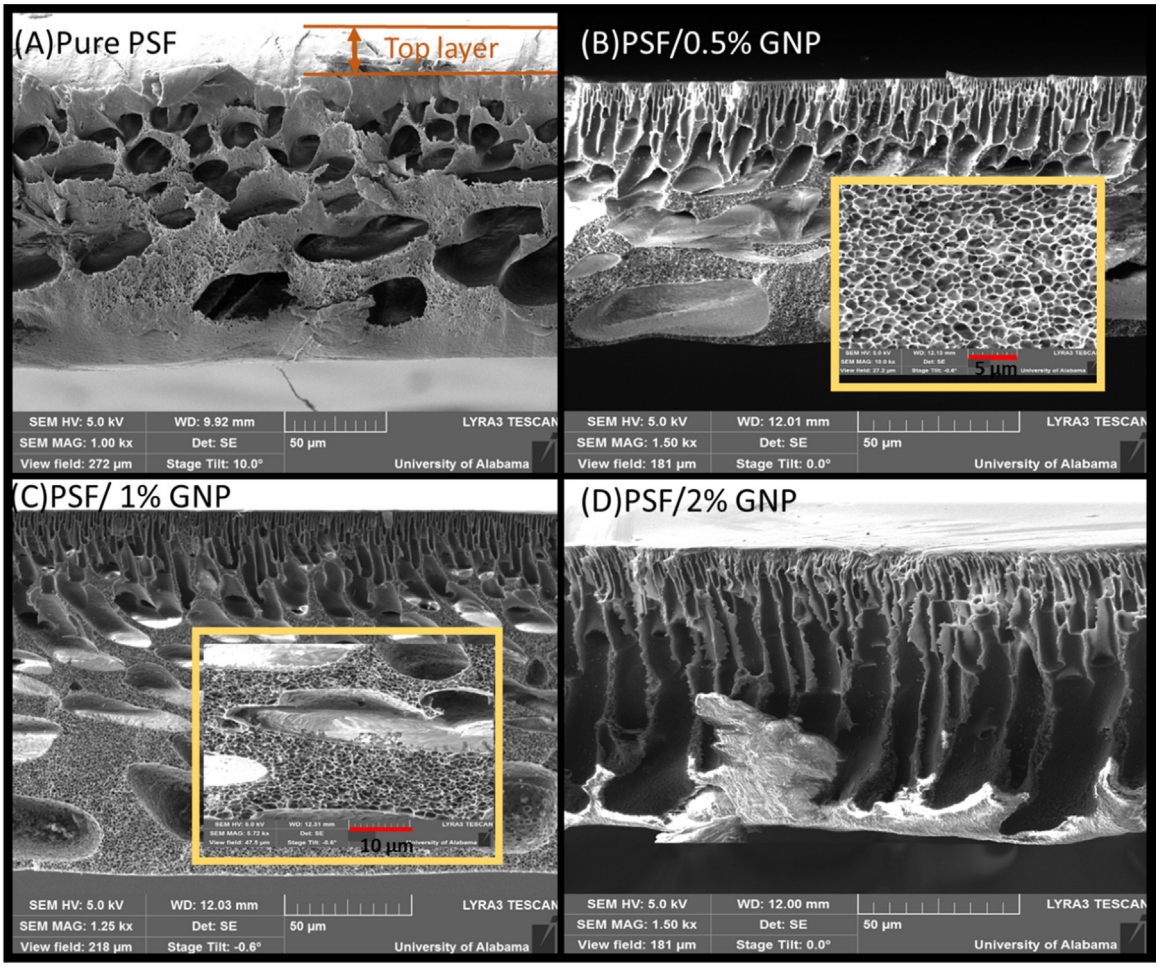

Fig. 2. SEM images of cross-section of a) pure PSF, b) PSF/0.5%GNP, c) PSF/1% GNP and d) PSF/2% GNP.

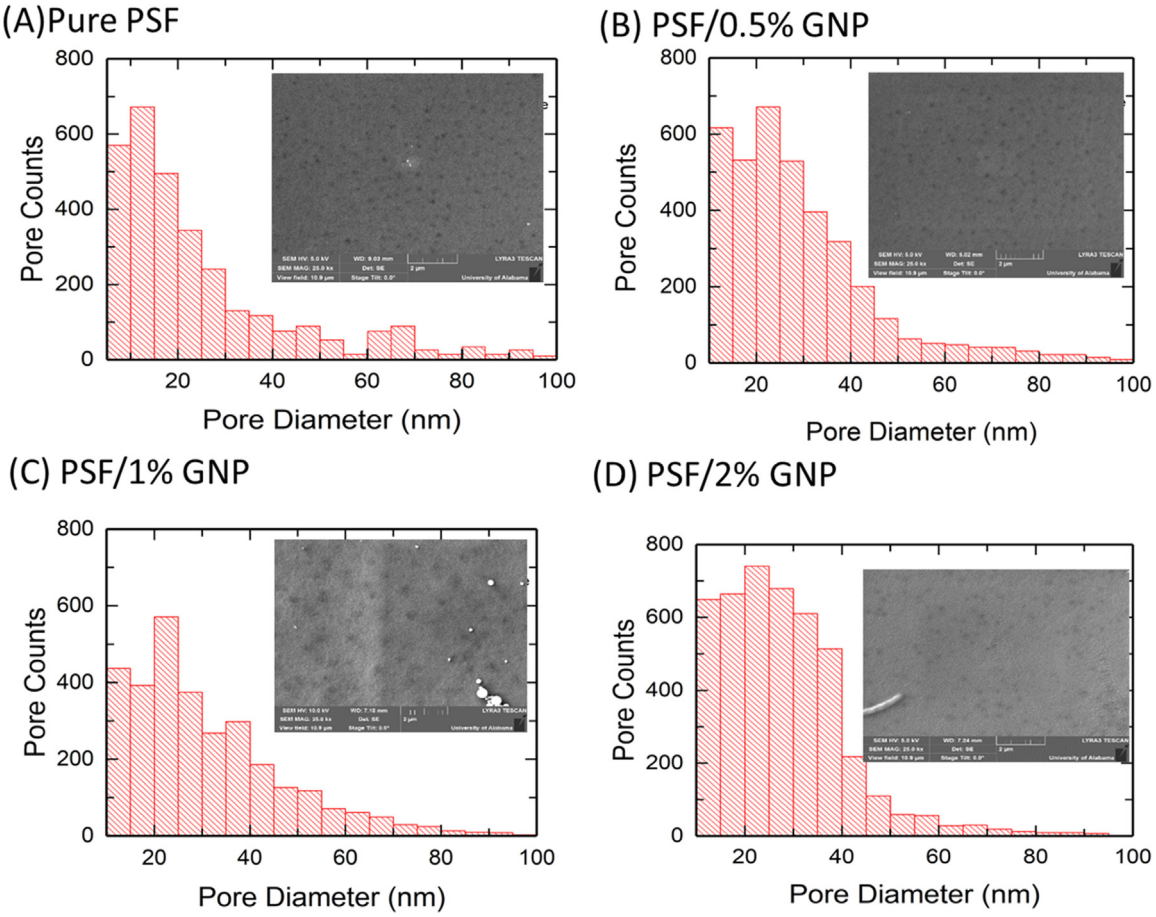

Fig. 3. SEM images and top surface pores analysis of a) pure PSF, b) PSF/0.5% GNP, c) PSF/1% GNP and d) PSF/2% GNP.

pore morphology [41–44]. The porosity of all the gold nanocomposite membranes (% 85 ± 5) was higher in comparison with porosity of pure PSF membranes (% 75 ± 5) [44].

The surface chemistry of the CT-gold nanocomposite membranes was evaluated using FTIR to investigate the linkage of the gold nanoparticles and polysulfone matrix (Fig. 4). All the membranes showed peaks around 1044 cm^{-1}, 1106 cm^{-1}, 1150 cm^{-1}, 1241 cm^{-1}, and 1488 cm^{-1} regarding to SO_3H, C—O, R(SO_2)—R, C—O, and aromatic bond representing the polysulfone structure characteristic peaks [45,46]. Peaks around ~3000 cm^{-1} are addressing the citrate coating on the GNP. The peak intensity enhancement at ~3000 cm^{-1} from PSF/0.5% GNP to PSF/1% GNP, and PSF/2% GNP membrane indicates the higher content of GNPs in the gold nanocomposite membranes, respectively [47,48]. Also, lower intensity of the peaks around ~1310, 1300, 800, 100 cm^{-1} in the PSF/1% GNP, and PSF/2% GNP membranes is a result of higher GNP interaction with the PSF matrix and a higher content of hydrogen bonds between the GNPs and PSF which proves the incorporation of GNPs into PSF membranes [49].

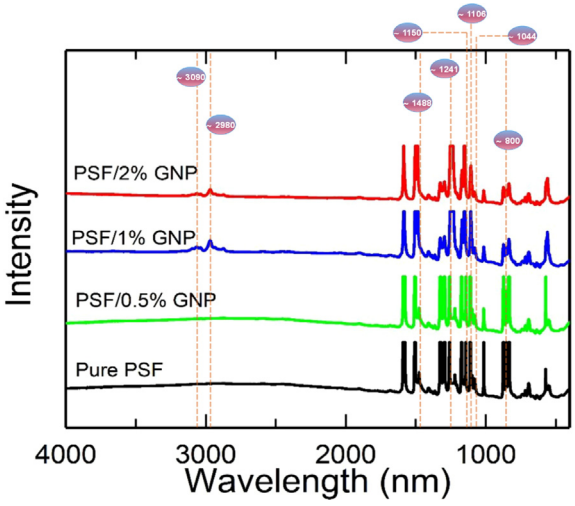

Fig. 4. FTIR spectroscopy of the pure PSF, PSF/0.5% GNP, PSF/1% GNP, and PSF/2% GNP.

Water contact angle (CA) measurement is the standard method to examine the surface hydrophilicity of membranes. Fig. 5 shows the dynamic and static contact angle of all the membranes. The static contact angle of all the gold nanocomposite membranes decreased significantly in comparison with the contact angle of pure PSF membranes. The CA did not change significantly by increasing the load of CT-GNPs into the membrane. That can be due to the aggregation of GNPs at higher concentrations and poor distribution on the surface of nanocomposite membranes [50]. Improvement of membrane hydrophilicity can be the result of different factors such as chemical compositional changes and structural changes [51,52]. The increased hydrophilicity of the gold nanocomposite membranes can be justified mainly due to the changes of hydrophilic constituents after addition of CT-GNPs into the PSF membranes. The hydrophilic functional groups of CT-GNPs are responsible for the new hydrophilic properties of gold nanocomposite membranes [53]. The dynamic CA shows the time dependence of water contact angle of the membranes. Water CA of the pure PSF membrane decreased slightly while those of gold nanocomposite membranes decreased rapidly with respect to the age of the drop. This behavior of gold nanocomposite membranes indicates that the addition of CT-GNP not only improved the surface hydrophilicity

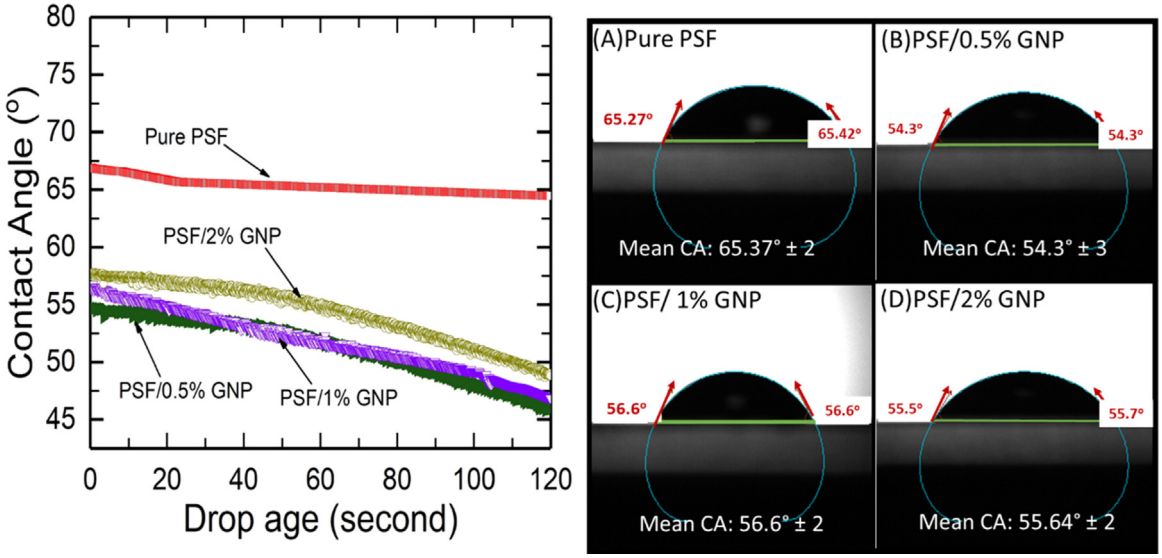

Fig. 5. Dynamic and static contact angle of pure PSF and gold nanocomposite membranes.

but also the hydrophilicity of pores inside the membrane [40].

The electrical surface charge of membranes plays an important role in flux and the antifouling ability of membranes. Fig. 6 displays the electrical surface charges of all the membranes measured at a pH range of 4–5, similar to the filtration pH range [22,54]. The electrical surface charges of membranes increased with the addition of gold nanoparticles content. As it was shown in Fig. 6(a), the citrate-coated gold nanoparticles have a negative surface charge due to the citrate functional groups. Therefore, the addition of CT-GNPs into the membrane surface enhanced the negative electrical surface charge of nanocomposite membranes.

3.2. Membrane performance

Fig. 7 shows the pure water flux of all the membranes at constant TMP = 0.16 MPa and cross-flow velocity of 0.16 m s^{-1}. The enhanced water fluxes of the gold nanocomposite membranes were expected based on the improved structural and physicochemical properties of the gold nanocomposite membranes that were discussed above. The PSF/0.5% GNP and PSF/1% GNP nanocomposite membranes showed three times higher fluxes when compared with the pure PSF stable water flux. This improved permeation behavior can be explained by the fact that PSF/0.5% GNP and PSF/1% GNP nanocomposite membranes possess higher porosity, more finger-like connected pores (Fig. 2), and higher hydrophilicity (Fig. 5). The mentioned optimal structural and surface chemistry properties reduce the resistance of water permeating through

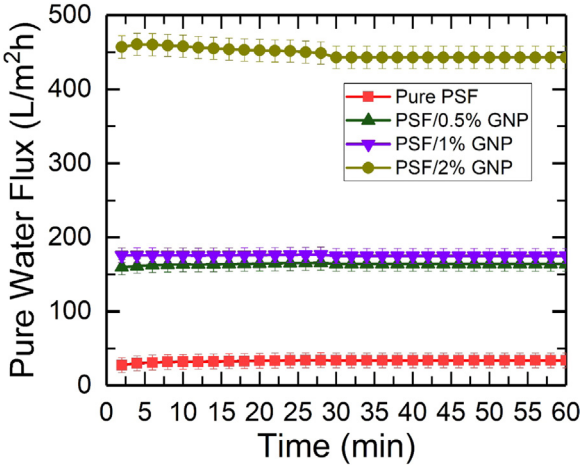

Fig. 7. Pure water flux of pure PSF and gold nanocomposite membranes at TMP = 0.16 MPa and cross-flow velocity of 0.16 m s^{-1}.

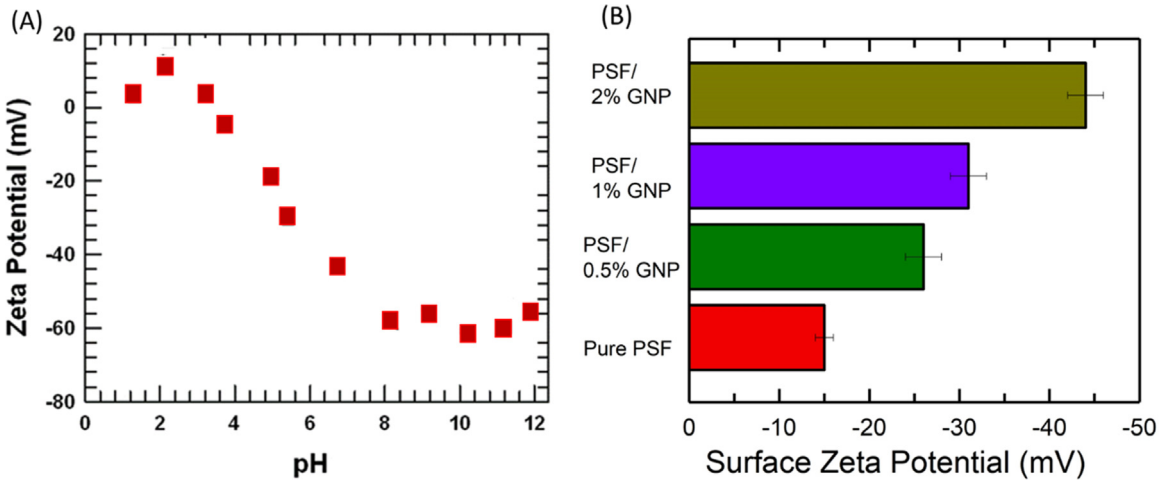

Fig. 6. (a) Zeta potential of CT-GNP across a pH range, (b) Zeta potential of PSF and gold nanocomposite membranes at pH = 4–5.

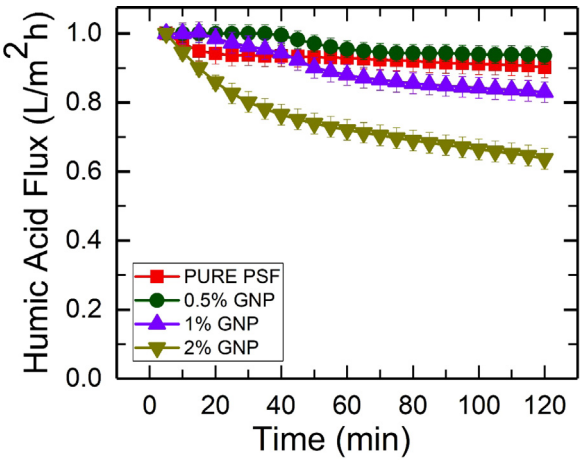

Fig. 8. Humic acid (10 ppm) flux for pure PSF and gold nanocomposite membranes at TMP = 0.16 MPa and cross-flow velocity of 0.16 m s^{-1}.

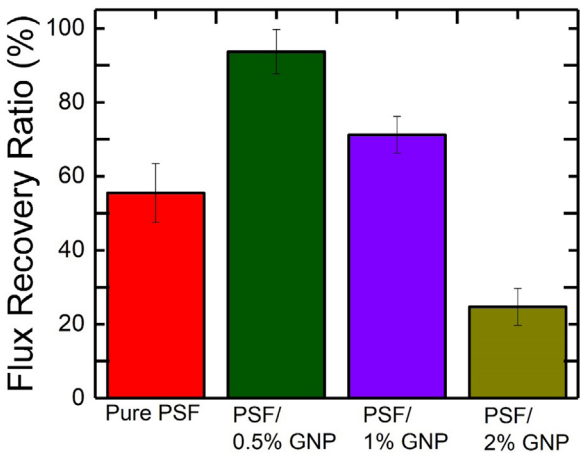

Fig. 9. Pure water flux recovery ratio for 10 ppm HA solution at TMP = 0.16 MPa and cross-flow velocity of 0.16 m s^{-1}.

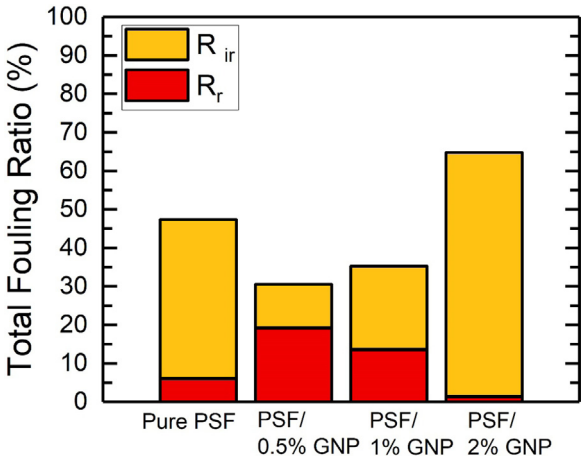

Fig. 10. Fouling ratio of all membranes after filtration of 10 ppm HA solution at TMP = 0.16 MPa and cross-flow velocity of 0.16 m s^{-1}.

the membrane pores and therefore increase membrane permeability [40,55]. The enhanced flux behavior was more significant for PSF/2% GNP nanocomposite membranes; pure water flux increased to around 450 L m^{-2} h^{-1} in comparison with pure water flux of pure PSF membranes of 50 L m^{-2} h^{-1}. This sharp flux increase may be justified based on the facilitated water molecules transport due to the larger surface pore sizes and long channel shape pores that connected the top surface of the membrane to the bottom surface with low tortuosity, which therefore alleviated transport resistance [56]. Fig. 8 shows the flux decline behavior of all the membranes during the 10 ppm HA filtration at a cross-flow velocity of 16 m s^{-1}. The PSF/2% GNP nanocomposite membranes showed the highest flux reduction (40% flux reduction), by rapid reduction after a few minutes of HA filtration. The large surface pore sizes of PSF/2% GNP nanocomposite membranes could be easily occupied by the entrance of HA particles into the pores and started the internal pore blocking. This phenomenon can be assigned as the main reason for flux reduction. The PSF/1% GNP nanocomposite membranes showed better antifouling behavior compared to the pure PSF membranes for the first 40 min of HA filtration with less than 10% flux reduction. However, the HA flux reduced to 15% of the initial flux after 40 min of filtration. This dynamic behavior can be justified based on the two main characteristics of the PSF/1% GNP nanocomposite membranes. First, the higher hydrophilicity (Fig. 5) and higher negative surface electrical charge (Fig. 6) provided facilitated transport of water molecules through the pores and with regard to the negative surface charge of HA, enhanced negative-negative (membrane surface-HA compounds) repulsion [57]. However, after 40 min of filtration, due to the larger pore sizes of PSF/1% GNPs compared to the pure PSF, the formation of a HA cake layer on the surface and into the pores overcame the surface charge repulsion and fouling initiated that resulted in flux decline. PSF/0.5% GNP nanocomposite membranes exhibited the best flux retention during 120 min of HA filtration with less than 5% flux reduction. The combination of optimal pore size, interconnected pore structure, high hydrophilicity and negative surface charge can be named as the main factors of enhanced antifouling capability of PSF/0.5% GNP nanocomposite membranes. The FRR% data completes the nanocomposite anti-fouling behavior assessment. In general, fouling is categorized to reversible and irreversible fouling. Reversible fouling is attributed to the deposition of particles on the membrane surface (cake layer formation) which can be removed from the surface by water flushing that resulted in high FRR%. Irreversible fouling is attributed to the adsorption of particles into the surface and pores (internal pore blocking) which cannot be removed by water flushing that resulted in low FRR%, and other chemical, physical or enzymatic methods are needed to clean the membrane [58]. Fig. 9 shows that PSF/0.5% GNP and PSF/1% GNP nanocomposite membranes showed the highest (93% and 75%, respectively) FRR% among all the membranes. This behavior can be explained by that fact that the hydrophilic surface of those membranes provides the smoother environment for water molecules transportation via hydrogen bonding as well as less adsorption of HA molecules into the surface. The large surface pores of nanocomposite membranes that convey larger quantities of water suffer from rapid internal pore blocking by HA particles in comparison with smaller surface pores [59,60]. The effect of pore size on the trade-off between the high pure water flux and low FRR% can be seen in PSF/2% GNP nanocomposite that showed the highest pure water flux and the highest HA flux decline as well as lowest FRR%. These results can be justified by the fact the large surface pore sizes of PSF/2% GNP lead to internal blocking by the HA particles and could not be cleaned by water flushing. The fouling ratio was calculated for better assessment of membranes fouling behavior (Fig. 10). The fouling reversibility increased for PSF/0.5% GNP and PSF/1% GNP nanocomposite membranes in comparison with pure PSF membrane. However, PSF/2% GNP nanocomposite membranes encountered the irreversible fouling due to large surface pore size and vertical pore structure as it was discussed earlier. The highest fouling reversibility belongs to the PSF/0.5% GNP nanocomposite membranes. This self-cleaning capability can be explained based on the improved hydrophilicity and digestive behavior of CT-GNPs for HA molecules as it was discussed in the following section [36,61].

The CT-GNPs particle size and TEM images were shown in Fig. 11 [62]. The HA aggregation behavior was analyzed to evaluate the effect

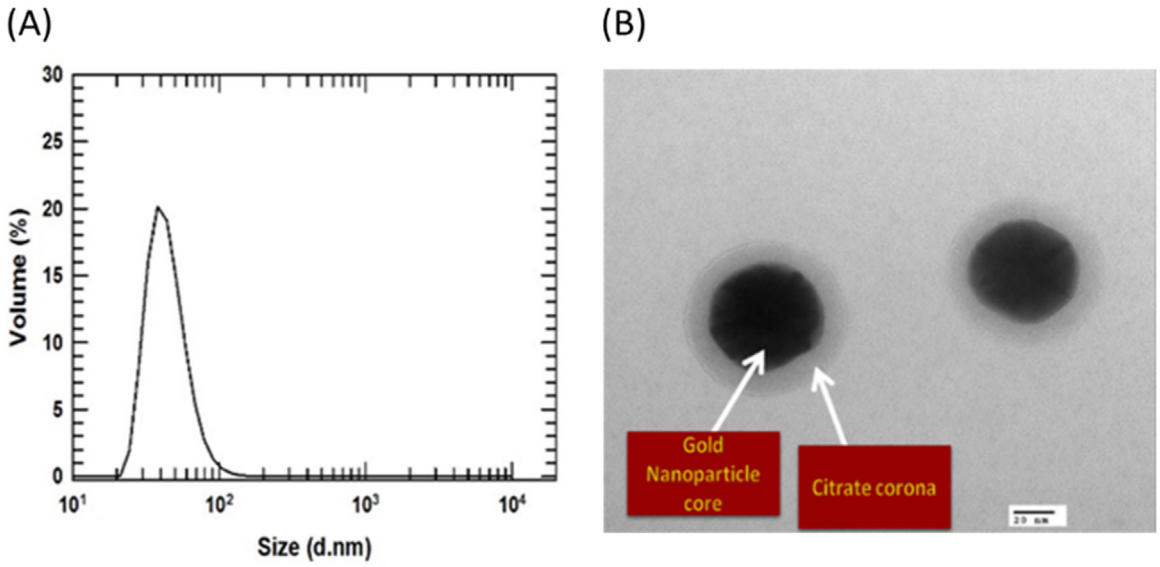

Fig. 11. (a) Particle size distribution of CT-GNP 50 nm, (b) Transmission electron microscopy (TEM) image of CT-GNP 50 nm.

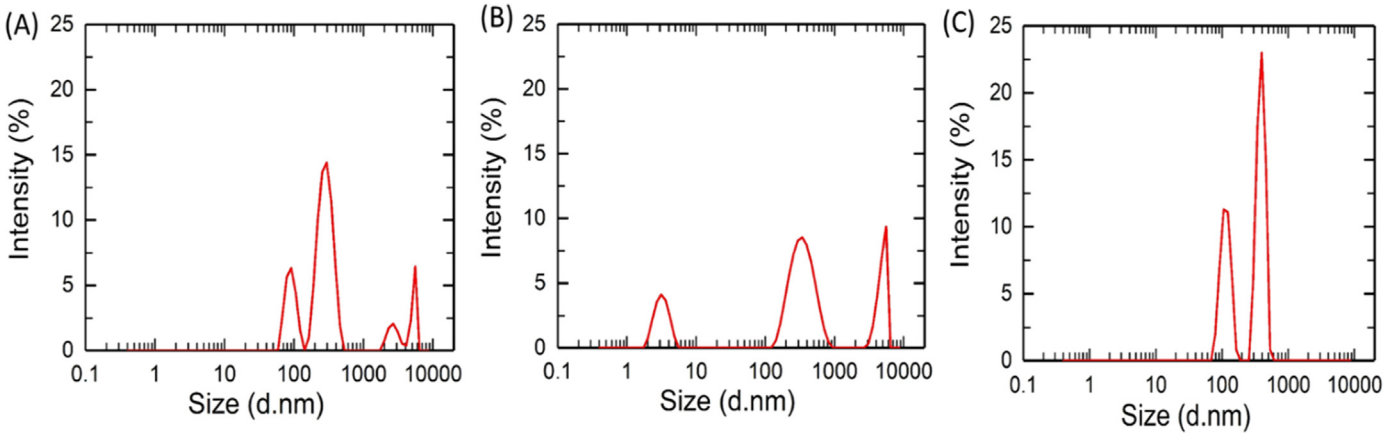

Fig. 12. Particle size distribution of HA at (a) 10 ppm feed solution, (b) permeate stream of pure PSF and (c) permeate stream of PSF/0.5 gold nanocomposite membranes. These plots are representative of HA particle size distribution for HA samples after 10, 30, and 60 min of filtrations. The error was less than 10% of the mean value.

of CT-GNPs on the interaction of HA aggregates with membranes surface and pores regarding the self-cleaning ability of gold nanocomposite membranes. The particle size distribution of HA feed solution and permeate stream of HA filtration were monitored after 10, 30 and 60 min of filtration for pure PSF membranes and gold nanocomposite membranes. The representative of at least 9 measurements was shown in Fig. 12. The HA feed solution showed three size generation of HA particles including 1) HA particle less than 100 nm, 2) HA aggregates larger than 100 nm and smaller than 1 μm, and 3) HA aggregates more than 1 μm and less than 10 μm (Fig. 12(a)). The observed HA particle size distribution agree with the dynamic aggregation behavior of HA reported by Esfahani et al., [24,36].The permeate stream of pure PSF membranes also showed the three size generation including the large aggregates between 1 and 10 μm (Fig. 12(b)). The comparison between HA aggregates size distribution in feed solution and permeate stream showed the existence of three size generation of HA aggregates. However, the permeate stream of the gold nanocomposite membranes showed only two size generations of HA with no aggregates larger than 1 μm (Fig. 12(c)). The absence of large aggregate size (> 1 μm) in the permeate stream of gold nanocomposite membranes, while those large HA aggregates observed in the permeate stream of pure PSF membranes at the same filtration conditions, indicates that gold embedded nanoparticles facilitated the disaggregation of HA aggregates and fragmented the HA aggregates larger than 1 μm. Since pure PSF and gold nanocomposite membranes showed the same top surface pore size ranges, therefore, this phenomenon could not be attributed to the sieving effect by the membranes. One possible explanation for this HA disaggregation is the modification of hydrogen bonds in the HA aggregates resulted from ligand exchange interaction between HA molecules and CT-GNPs [22]. The similar disaggregation of HA aggregates was reported by Piccolo et al. [63] and Brigante et al. [64] where the HA aggregates interact with monocarboxylic acids. They suggested that aggregation of humic substances (HS) is based on hydrophobic forces, and these forces can be disrupted when carboxylic acids interact with HS, resulting in smaller HS molecules and disaggregation of HS [22]. They postulated that carboxylic acid might interact with HA molecules, forming hydrogen bonds between HA molecules and carboxylic functionality. The newly formed bonds can modify existing hydrogen bonds between HA molecules and therefore alter the hydrophobic forces that hold the molecules together [22,63,64]. The obtained results of HA aggregate size in the permeate stream of gold nanocomposite membranes suggest a similar interaction between CT-GNPs on HA aggregates. The main benefits of this behavior can be seen in the self-cleaning ability of the gold nanocomposite membranes; disaggregation of HA aggregates loosens the cake layer attached on the membrane surface and opens the membrane pores, which were previously blocked

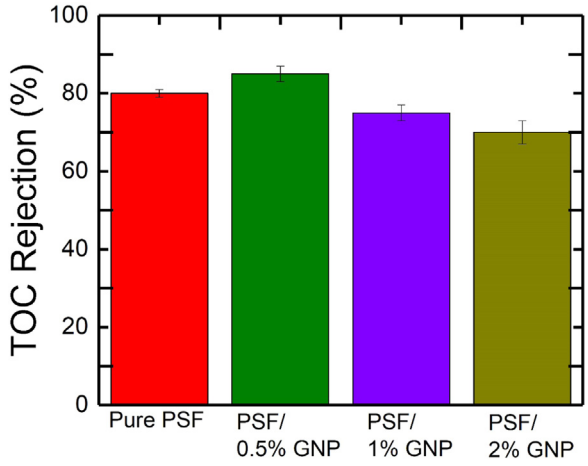

Fig. 13. Total organic carbon rejection of 10 ppm HA concentration by pure PSF and gold nanocomposite membranes. TMP = 0.16 MPa and cross-flow velocity is 0.16 m s^{-1}.

by large HA aggregates. The antifouling results of gold nanocomposite membranes suggest that behavior. The higher FRR% (Fig. 9), as well as the higher ratio of reversible fouling (Fig. 10) of 0.5% and 1% gold nanocomposites membranes in comparison with the pure PSF membranes with the same pore sizes can be attributed to the disaggregation of HA cake layer or HA aggregates in/on the pores that could be more easily removed by hydraulic water cleaning process.

The HA rejection capability of all the membranes at T = 25 °C and after two hours filtration is presented in Fig. 13. The membrane structure and electrical surface charge are the two main factors in the rejection process. The dense top layer results in poor permeability but high rejection, while the porous top layer results in enhanced permeability and low rejection [65]. In addition, as the HA particles have a negative surface charge, a higher negative surface charge of membranes enhances the negative-negative repulsion between HA and membrane surface, resulting in higher rejection [66]. The PSF/0.5% GNP nanocomposite membranes exhibited the highest rejection, at 87%, among all membranes. This promising ability can be attributed to the enhanced negative electrical surface charge and enhanced the hydrophilicity of PSF/0.5% GNP nanocomposite membranes [67,68]. The PSF/2% GNP nanocomposite membranes showed the lowest rejection among all the membranes, which is due to the large pore sizes where HA particles could easily pass through. Although the PSF/2% GNP possesses the highest negative surface charge among the membranes, these results indicate that pore size is a more influential factor when compared to the membrane surface charge.

An important practical aspect of nanocomposite membranes is durability and stability of embedded nanoparticles inside the membranes. The long-term stability of gold nanoparticles inside the PSF membranes were investigated at static and dynamic conditions. In the static condition, the release of CT-GNPs from gold nanocomposite membranes was monitored by tracking the presence of GNPs in the container that stored the membranes in DI water for more than three months. The UV–Vis spectra of the samples did not show any release of CT-GNPs for all the gold nanocomposite membranes (Fig. 14). No sign of CT-GNPs leaching was observed when tested under dynamic conditions. While running seven days of filtration tests at TMPs of 0.16 MPa and 0.3 MPa and cross-flow velocity of 0.16 m s^{-1}, no CT-GNPs were found in the permeate stream of gold nanocomposite membranes. This data indicates that the CT-GNPs were immobilized firmly inside the PSF polymeric matrix.

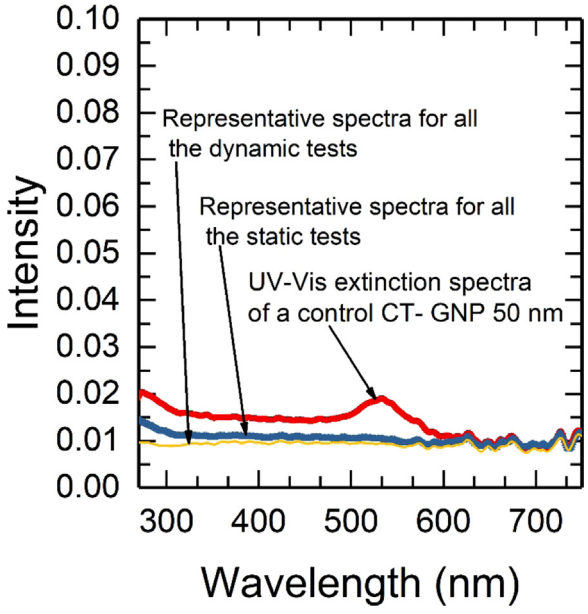

Fig. 14. UV–Vis extinction spectra of: control CT-GNPs 50 nm, representative data of static release experiments for three months and representative data of dynamic (filtration) release experiments for seven days. Note: representative data shows one plot where the results of several samples overlapped each other.

4. Conclusions

CT-GNPs having 50 nm size possess negative surface charge and hydrophilic functional groups with degrading ability towards HA aggregates. CT-GNPs have shown noticeable effects on antifouling ability of PSF membranes. The results showed that the loading of GNPs affected the pore structure and morphology of PSF membranes differently. The main reason for this behavior could be attributable to the aggregation of CT-GNPs and different distribution patterns in the polymeric matrix. The PSF/0.5% gold nanocomposite membranes showed the optimal physicochemical properties and performance with enhanced permeation (160 L m^{-2} h^{-1}, three times higher than pure PSF), the highest HA rejection (87%), enhanced antifouling, and the highest FRR (95%) among all membranes. The major conclusions from the current study suggest that CT-GNPs affected the trade-off relationship between permeability, selectivity and antifouling capability of membranes symmetrically, without compromising any aspects of the membrane process. The hydrophilic functional groups and negative surface charges of CT-GNPs enhanced the permeation and rejection capability of nanocomposite membranes, and the CT-GNPs aid in disaggregation of HA in water solution at room temperature and under regular visible light improved the self-cleaning behavior of nanocomposite membranes. The digestive antifouling behavior of gold nanocomposite membranes facilitated the cleaning process of membranes by degrading the formed HA cake layer on the membrane surface and fragmenting the large HA aggregates stuck inside the membrane pores. The gold nanocomposite membranes showed no leaching of embedded CT-GNPs under the dynamic and static release experiments across several days and months, respectively.

Acknowledgment

The authors thank Dr. Holly A. Stretz and Dr. Martha J.M. Wells at the Tennessee Technological University for useful discussions regarding the gold nanoparticles properties. The authors gratefully thank the Department of Chemical and Biological Engineering at the University of Alabama and the Center for the Management, Utilization, and Protection of Water Resources at the Tennessee Technological

University.

References

[1] A. Mollahosseini, A. Rahimpour, M. Jahamshahi, M. Peyravi, M. Khavarpour, The effect of silver nanoparticle size on performance and antibacteriality of polysulfone ultrafiltration membrane, Desalination 306 (2012) 41–50.

[2] N. Koutahzadeh, M.R. Esfahani, P.E. Arce, Removal of acid black 1 from water by the pulsed corona discharge advanced oxidation method, J. Water Process Eng. 10 (2016) 1–8.

[3] M.M. Pendergast, E.M. Hoek, A review of water treatment membrane nanotechnologies, Energy Environ. Sci. 4 (2011) 1946–1971.

[4] M.-C. Daniel, D. Astruc, Gold nanoparticles: assembly, supramolecular chemistry, quantum-size-related properties, and applications toward biology, catalysis, and nanotechnology, Chem. Rev. 104 (2004) 293–346.

[5] G. Xue, H. Liu, Q. Chen, C. Hills, M. Tyrer, F. Innocent, Synergy between surface adsorption and photocatalysis during degradation of humic acid on TiO2/activated carbon composites, J. Hazard. Mater. 186 (2011) 765–772.

[6] H. Basri, A.F. Ismail, M. Aziz, Polyethersulfone (PES)–silver composite UF membrane: effect of silver loading and PVP molecular weight on membrane morphology and antibacterial activity, Desalination 273 (2011) 72–80.

[7] M. Zhu, H. Wang, A.A. Keller, T. Wang, F. Li, The effect of humic acid on the aggregation of titanium dioxide nanoparticles under different pH and ionic strengths, Sci. Total Environ. 487 (2014) 375–380.

[8] J. Shao, J. Hou, H. Song, Comparison of humic acid rejection and flux decline during filtration with negatively charged and uncharged ultrafiltration membranes, Water Res. 45 (2011) 473–482.

[9] G. Chen, X. Liu, C. Su, Distinct effects of humic acid on transport and retention of TiO2 rutile nanoparticles in saturated sand columns, Environ. Sci. Technol. 46 (2012) 7142–7150.

[10] M.D. Firouzjaei, A.A. Shamsabadi, M. Sharifian Gh, A. Rahimpour, M. Soroush, A novel nanocomposite with superior antibacterial activity: a silver-based metal organic framework embellished with graphene oxide, Adv. Mater. Interfaces (2018) 1701365.

[11] L. Liang, L. Luo, S. Zhang, Adsorption and desorption of humic and fulvic acids on SiO2 particles at nano-and micro-scales, Colloids Surf. A: Physicochem. Eng. Asp. 384 (2011) 126–130.

[12] H. Niu, D. Zhang, S. Zhang, X. Zhang, Z. Meng, Y. Cai, Humic acid coated Fe3O4 magnetic nanoparticles as highly efficient Fenton-like catalyst for complete mineralization of sulfathiazole, J. Hazard. Mater. 190 (2011) 559–565.

[13] J.-H. Li, X.-S. Shao, Q. Zhou, M.-Z. Li, Q.-Q. Zhang, The double effects of silver nanoparticles on the PVDF membrane: surface hydrophilicity and antifouling performance, Appl. Surf. Sci. 265 (2013) 663–670.

[14] S.H. Kim, S.-Y. Kwak, B.-H. Sohn, T.H. Park, Design of TiO2 nanoparticle self-assembled aromatic polyamide thin-film-composite (TFC) membrane as an approach to solve biofouling problem, J. Membr. Sci. 211 (2003) 157–165.

[15] J. Yin, B. Deng, Polymer-matrix nanocomposite membranes for water treatment, J. Membr. Sci. 479 (2015) 256–275.

[16] A. Zirehpour, A. Rahimpour, S. Khoshhal, M.D. Firouzjaei, A.A. Ghoreyshi, The impact of MOF feasibility to improve the desalination performance and antifouling properties of FO membranes, RSC Adv. 6 (2016) 70174–70185.

[17] A. Rahimpour, S.F. Seyedpour, S. Aghapour Aktij, M. Dadashi Firouzjaei, A. Zirehpour, A. Arabi Shamsabadi, S. Khoshhal Salestan, M. Jabbari, M. Soroush, Simultaneous improvement of antimicrobial, antifouling, and transport properties of forward osmosis membranes with immobilized highly-compatible polyrhodanine nanoparticles, Environ. Sci. Technol. 52 (2018) 5246–5258.

[18] K. Zodrow, L. Brunet, S. Mahendra, D. Li, A. Zhang, Q. Li, P.J. Alvarez, Polysulfone ultrafiltration membranes impregnated with silver nanoparticles show improved biofouling resistance and virus removal, Water Res. 43 (2009) 715–723.

[19] I. Vikholm-Lundin, E. Rosqvist, P. Ihalainen, T. Munter, A. Honkimaa, V. Marjomäki, W.M. Albers, J. Peltonen, Assembly of citrate gold nanoparticles on hydrophilic monolayers, Appl. Surf. Sci. 378 (2016) 519–529.

[20] P.K. Jain, X. Huang, I.H. El-Sayed, M.A. El-Sayed, Noble metals on the nanoscale: optical and photothermal properties and some applications in imaging, sensing, biology, and medicine, Acc. Chem. Res. 41 (2008) 1578–1586.

[21] V.L. Pallem, H.A. Stretz, M.J. Wells, Evaluating aggregation of gold nanoparticles and humic substances using fluorescence spectroscopy, Environ. Sci. Technol. 43 (2009) 7531–7535.

[22] M.R. Esfahani, V.L. Pallem, H.A. Stretz, M.J. Wells, Humic acid disaggregation with/of gold nanoparticles: effects of nanoparticle size and pH, Environ. Nanotechnol. Monit. Manag. 6 (2016) 54–63.

[23] M.R. Esfahani, V.L. Pallem, H.A. Stretz, M.J. Wells, Extinction, emission, and scattering spectroscopy of 5–50 nm citrate-coated gold nanoparticles: an argument for curvature effects on aggregation, Spectrochim. Acta Part A: Mol. Biomol. Spectrosc. 175 (2017) 100–109.

[24] M.R. Esfahani, V.L. Pallem, H.A. Stretz, M.J. Wells, Core-size regulated aggregation/disaggregation of citrate-coated gold nanoparticles (5–50 nm) and dissolved organic matter: extinction, emission, and scattering evidence, Spectrochim. Acta Part A: Mol. Biomol. Spectrosc. 189 (2018) 415–426.

[25] H. Lin, W. Peng, M. Zhang, J. Chen, H. Hong, Y. Zhang, A review on anaerobic membrane bioreactors: applications, membrane fouling and future perspectives, Desalination 314 (2013) 169–188.

[26] S. Hong, M. Elimelech, Chemical and physical aspects of natural organic matter (NOM) fouling of nanofiltration membranes, J. Membr. Sci. 132 (1997) 159–181.

[27] X. Cheng, H. Liang, A. Ding, X. Tang, B. Liu, X. Zhu, Z. Gan, D. Wu, G. Li, Ferrous iron/peroxymonosulfate oxidation as a pretreatment for ceramic ultrafiltration membrane: control of natural organic matter fouling and degradation of atrazine, Water Res. 113 (2017) 32–41.

[28] A. Matilainen, M. Vepsäläinen, M. Sillanpää, Natural organic matter removal by coagulation during drinking water treatment: a review, Adv. Colloid Interface Sci. 159 (2010) 189–197.

[29] N. Hamid, A. Ismail, T. Matsuura, A. Zularisam, W. Lau, E. Yuliwati, M. Abdullah, Morphological and separation performance study of polysulfone/titanium dioxide (PSF/TiO2) ultrafiltration membranes for humic acid removal, Desalination 273 (2011) 85–92.

[30] C.Y. Tang, Q. She, W.C. Lay, R. Wang, A.G. Fane, Coupled effects of internal concentration polarization and fouling on flux behavior of forward osmosis membranes during humic acid filtration, J. Membr. Sci. 354 (2010) 123–133.

[31] D.A. Giljohann, D.S. Seferos, W.L. Daniel, M.D. Massich, P.C. Patel, C.A. Mirkin, Gold nanoparticles for biology and medicine, Angew. Chem. Int. Ed. 49 (2010) 3280–3294.

[32] Y. Na, S. Yang, S. Lee, Evaluation of citrate-coated magnetic nanoparticles as draw solute for forward osmosis, Desalination 347 (2014) 34–42.

[33] M. Răcuciu, Synthesis protocol influence on aqueous magnetic fluid properties, Curr. Appl. Phys. 9 (2009) 1062–1066.

[34] T.E. Thomas, S. Al Aani, D.L. Oatley-Radcliffe, P.M. Williams, N. Hilal, Laser Doppler electrophoresis and electro-osmotic flow mapping: a novel methodology for the determination of membrane surface zeta potential, J. Membr. Sci. 523 (2017) 524–532.

[35] N.A. Hashim, Y. Liu, K. Li, Preparation of PVDF hollow fiber membranes using SiO2 particles: the effect of acid and alkali treatment on the membrane performances, Ind. Eng. Chem. Res. 50 (2011) 3035–3040.

[36] M.R. Esfahani, H.A. Stretz, M.J. Wells, Abiotic reversible self-assembly of fulvic and humic acid aggregates in low electrolytic conductivity solutions by dynamic light scattering and zeta potential investigation, Sci. Total Environ. 537 (2015) 81–92.

[37] M.R. Esfahani, E.M. Languri, M.R. Nunna, Effect of particle size and viscosity on thermal conductivity enhancement of graphene oxide nanofluid, Int. Commun. Heat. Mass Transf. 76 (2016) 308–315.

[38] N. Koutahzadeh, M.R. Esfahani, F. Bailey, A. Taylor, A.R. Esfahani, Enhanced performance of polyhedral oligomeric silsesquioxanes /polysulfone nanocomposite membrane with improved permeability and antifouling properties for water treatment, J. Environ. Chem. Eng. Accept. (2018) JECE2597.

[39] E. Fontananova, J.C. Jansen, A. Cristiano, E. Curcio, E. Drioli, Effect of additives in the casting solution on the formation of PVDF membranes, Desalination 192 (2006) 190–197.

[40] S. Zhao, Z. Wang, X. Wei, B. Zhao, J. Wang, S. Yang, S. Wang, Performance improvement of polysulfone ultrafiltration membrane using well-dispersed polyaniline–poly (vinylpyrrolidone) nanocomposite as the additive, Ind. Eng. Chem. Res. 51 (2012) 4661–4672.

[41] C. Smolders, A. Reuvers, R. Boom, I. Wienk, Microstructures in phase-inversion membranes. Part 1. formation of macrovoids, J. Membr. Sci. 73 (1992) 259–275.

[42] M.-J. Han, S.-T. Nam, Thermodynamic and rheological variation in polysulfone solution by PVP and its effect in the preparation of phase inversion membrane, J. Membr. Sci. 202 (2002) 55–61.

[43] M.R. Esfahani, J.L. Tyler, H.A. Stretz, M.J. Wells, Effects of a dual nanofiller, nano-TiO 2 and MWCNT, for polysulfone-based nanocomposite membranes for water purification, Desalination 372 (2015) 47–56.

[44] Y. Yang, H. Zhang, P. Wang, Q. Zheng, J. Li, The influence of nano-sized TiO2 fillers on the morphologies and properties of PSF UF membrane, J. Membr. Sci. 288 (2007) 231–238.

[45] Y.T. Chung, L.Y. Ng, A.W. Mohammad, Sulfonated-polysulfone membrane surface modification by employing methacrylic acid through UV-grafting: optimization through response surface methodology approach, J. Ind. Eng. Chem. 20 (2014) 1549–1557.

[46] G.R. Guillen, T.P. Farrell, R.B. Kaner, E.M. Hoek, Pore-structure, hydrophilicity, and particle filtration characteristics of polyaniline–polysulfone ultrafiltration membranes, J. Mater. Chem. 20 (2010) 4621–4628.

[47] M. Doyen, K. Bartik, G. Bruylants, UV–Vis and NMR study of the formation of gold nanoparticles by citrate reduction: Observation of gold–citrate aggregates, J. Colloid Interface Sci. 399 (2013) 1–5.

[48] J.-W. Park, J.S. Shumaker-Parry, Structural study of citrate layers on gold nanoparticles: role of intermolecular interactions in stabilizing nanoparticles, J. Am. Chem. Soc. 136 (2014) 1907–1921.

[49] T. Fornaro, D. Burini, M. Biczysko, V. Barone, Hydrogen-bonding effects on infrared spectra from anharmonic computations: uracil–water complexes and uracil dimers, J. Phys. Chem. A 119 (2015) 4224–4236.

[50] M. Le Hir, Y. Wyart, G. Georges, L. Siozade, P. Sauvade, P. Moulin, Effect of salinity and nanoparticle polydispersity on UF membrane retention fouling, J. Membr. Sci. (2018).

[51] H. Susanto, M. Ulbricht, Characteristics, performance and stability of polyethersulfone ultrafiltration membranes prepared by phase separation method using different macromolecular additives, J. Membr. Sci. 327 (2009) 125–135.

[52] J.B. Li, J.W. Zhu, M.S. Zheng, Morphologies and properties of poly (phthalazinone ether sulfone ketone) matrix ultrafiltration membranes with entrapped TiO2 nanoparticles, J. Appl. Polym. Sci. 103 (2007) 3623–3629.

[53] K. Park, E.-J. Park, I.K. Chun, K. Choi, S.H. Lee, J. Yoon, B.C. Lee, Bioavailability and toxicokinetics of citrate-coated silver nanoparticles in rats, Arch. Pharmacal Res. 34 (2011) 153–158.

[54] Z. Zhou, Y. Yang, X. Li, W. Gao, H. Liang, G. Li, Coagulation efficiency and flocs characteristics of recycling sludge during treatment of low temperature and micro-polluted water, J. Environ. Sci. 24 (2012) 1014–1020.

[55] N. Koutahzadeh, M.R. Esfahani, H.A. Stretz, P.E. Arce, Investigation of UV/H2O2 pretreatment effects on humic acid fouling on polysulfone/titanium dioxide—and polysulfone/multiwall carbon nanotube—nanocomposite ultrafiltration membranes, Environ. Prog. Sustain. Energy 36 (2017) 27–37.
[56] A.K. Ghosh, E.M. Hoek, Impacts of support membrane structure and chemistry on polyamide–polysulfone interfacial composite membranes, J. Membr. Sci. 336 (2009) 140–148.
[57] Q. Liu, S. Huang, Y. Zhang, S. Zhao, Comparing the antifouling effects of activated carbon and TiO2 in ultrafiltration membrane development, J. Colloid Interface Sci. 515 (2018) 109–118.
[58] M.R. Esfahani, H.A. Stretz, M.J. Wells, Comparing humic acid and protein fouling on polysulfone ultrafiltration membranes: adsorption and reversibility, J. Water Process Eng. 6 (2015) 83–92.
[59] C.-W. Li, Y.-S. Chen, Fouling of UF membrane by humic substance: effects of molecular weight and powder-activated carbon (PAC) pre-treatment, Desalination 170 (2004) 59–67.
[60] I.N.H.M. Amin, A.W. Mohammad, M. Markom, L.C. Peng, N. Hilal, Flux decline study during ultrafiltration of glycerin-rich fatty acid solutions, J. Membr. Sci. 351 (2010) 75–86.
[61] N. Koutahzadeh, M.R. Esfahani, P.E. Arce, Sequential use of UV/H2O2—(PSF/TiO2/MWCNT) Mixed matrix membranes for dye removal in water purification: membrane permeation, fouling, rejection, and decolorization, Environ. Eng. Sci. (2016).
[62] V.L. Pallem, Fate and transformation of gold nanoparticles in surface water conditions, in, 2011.
[63] A. Piccolo, P. Conte, A. Cozzolino, Effects of mineral and monocarboxylic acids on the molecular association of dissolved humic substances, Eur. J. Soil Sci. 50 (1999) 687–694.
[64] M. Brigante, G. Zanini, M. Avena, On the dissolution kinetics of humic acid particles: effects of pH, temperature and Ca2+ concentration, Colloids Surf. A: Physicochem. Eng. Asp. 294 (2007) 64–70.
[65] K. Zhu, S. Zhang, J. Luan, Y. Mu, Y. Du, G. Wang, Fabrication of ultrafiltration membranes with enhanced antifouling capability and stable mechanical properties via the strategies of blending and crosslinking, J. Membr. Sci. 539 (2017) 116–127.
[66] D. Li, Y. Yan, H. Wang, Recent advances in polymer and polymer composite membranes for reverse and forward osmosis processes, Prog. Polym. Sci. 61 (2016) 104–155.
[67] B. Ganesh, A.M. Isloor, A.F. Ismail, Enhanced hydrophilicity and salt rejection study of graphene oxide-polysulfone mixed matrix membrane, Desalination 313 (2013) 199–207.
[68] C. Bellona, J.E. Drewes, The role of membrane surface charge and solute physicochemical properties in the rejection of organic acids by NF membranes, J. Membr. Sci. 249 (2005) 227–234.